Climate Dynamics
https://doi.org/10.1007/s00382-022-06595-5

The performance of CMIP6 models in simulating surface energy fluxes over global continents

Su Liu[1,2] · Zhu Liu[1,2,3] · Qingyun Duan[1,2,3] · Bohan Huang[1,2]

Received: 24 August 2022 / Accepted: 12 November 2022

Abstract
Correct simulation of land surface energy balance is critically important in reliably projecting future climate change. In this study, simulated surface energy fluxes including net radiation, latent heat, and sensible heat from 22 CMIP6 models are evaluated against ERA5 reanalysis data during 1950–2014 over global land surface to assess the performance of CMIP6 models in simulating surface energy balance. Results reveal significant differences in seasonal and regional characteristics of CMIP6 model simulations in the surface energy flux predictions. Net radiation is slightly overestimated in JJA (June, July, August) but underestimated in DJF (December, January, and February). Most models overestimate net radiation in both seasons over Africa, Australia, and Latin America. The inter-model variability of biases is substantial in DJF net radiation simulations over Asia, Europe and Siberia, and North America, although there is a good agreement between simulations of selected models and the ERA5 reanalysis data in JJA except for Greenland. Moreover, models overestimate latent heat and underestimate sensible heat in DJF, although latent heat and sensible heat simulations match well with the reference values in JJA. Latent heat is overestimated in DJF over Australia, Europe and Siberia, and Latin America. Sensible heat is underestimated during DJF over Europe and Siberia and Latin America. The performance of CMIP6 in Rn simulation is better than LH simulation and SH simulation for both JJA and DJF. Findings from this study will provide useful references for surface energy data users and future model development.

Keywords Model bias · Surface energy flux · CMIP6 · Seasonal pattern · Net radiation · Energy partition

1 Introduction

The evolution of climate is largely constrained by the global energy balance and its spatio-temporal variations (Ceppi and Gregory 2019; Huber and Knutti 2012; Stephens et al. 2012; Trenberth et al. 2009; Wild 2020). The global energy balance not only regulates the fundamental thermal conditions on Earth but also controls various atmosphere and land surface processes including atmospheric and oceanic circulation, hydrological cycle, glacier melting, plant productivity, and terrestrial carbon uptake (Kato et al. 2018; Wild et al. 2013). The amount of solar radiation reaching the surface of Earth largely according to the Sun-Earth geometry and changes with atmospheric composition, cloud amount, and water vapor content with the maximum absorption in the tropics (Trenberth and Fasullo 2013a, 2013b; Trenberth et al. 2015). Comparatively, the outgoing thermal radiation from the Earth's surface to the air is more uniformly distributed with latitude, which results in spatio-temporal variations of energy balance (Trenberth et al. 2015). The surface net radiation is the balance between incoming solar radiation and outgoing thermal radiation at the Earth's surface, which provides the basic driving force for the land surface processes and evolution of the ecological environment (Mauder et al. 2020). In addition, net radiation is also very important in the surface energy balance, which controls the partitioning of sensible heat flux, latent heat flux, and

Su Liu and Zhu Liu are co-first authors and contributed equally to the work.

✉ Qingyun Duan
qyduan@hhu.edu.cn

[1] State Key Laboratory of Hydrology-Water Resources and Hydraulic Engineering, Hohai University, Nanjing, China

[2] College of Hydrology and Water Resources, Hohai University, Nanjing, China

[3] CMA-HHU Joint Laboratory for Hydrometeorological Studies, Hohai University, Nanjing, China

Published online: 27 November 2022

ground heat flux (Conte et al. 2019; Martens et al. 2020; Mauder et al. 2020). Surface energy partitioning modulates the thermodynamics and atmospheric circulation, which has a strong relationship with the occurrence and development of extreme events such as droughts and heatwaves (Hirschi et al. 2011; Li et al. 2021; Miralles et al. 2014; Ukkola et al. 2018).

Knowledge of the energy exchange at the top of the atmosphere (TOA) has been improved through satellite missions such as the Clouds and the Earth's Radiant Energy System and the Solar Radiation and Climate Experiment, which could accurately capture the radiation flux at TOA (Loeb et al. 2018; Stephens et al. 2012; Wielicki et al. 1996). However, the energy balance at the Earth's surface especially its seasonal and regional characteristics still needs further investigation since surface energy flux cannot be directly measured by satellites and it has to be inferred from the measurable TOA radiances through empirical or physical models (Wang et al. 2021). Model simulations are subject to bias since uncertainties exist in model structure, model parameterization, input variables, boundary conditions, and simplifying assumptions (AghaKouchak and Mehran 2013; Liu and Merwade 2018, 2019; Ukkola et al. 2020; Yin et al. 2021; You et al. 2021). Therefore, assessing the estimation accuracy of surface energy balance components is very crucial for correctly understanding the mechanism of the energy cycles on the Earth system and the land–atmosphere interactions (Dickinson 1995). The new generation of Coupled Model Inter-comparison Project Phase 6 (CMIP6) is currently available and provides the main scientific basis for the Sixth Assessment Report of the Intergovernmental Panel on Climate Change (IPCC AR6). Compared with CMIP5, CMIP6 models have shown significant improvements in spatial resolution, physical parameterizations and inclusion of additional earth system processes such as nutrient limitations on the terrestrial carbon cycle and ice sheets (Eyring et al. 2016; Liu et al. 2021, 2022a, b; Liu et al. 2014; Shu et al. 2020; Tian and Dong 2020). Additionally, CMIP6 models also account for atmospheric attenuation and emission and provide unprecedented details in estimations of surface energy components, which offers a great opportunity to revisit and evaluate the spatio-temporal variations of energy balance at the Earth's surface (Pendergrass 2020).

In this study, net radiation (calculated from upward shortwave radiation, downward shortwave radiation, upward longwave radiation, downward longwave radiation), latent heat and sensible heat predictions from 22 CMIP6 models are evaluated with ERA5 reanalysis data during 1950–2014 over global land surface as well as six continents. We evaluate the model prediction bias in different seasons to understand: (1) how CMIP6 models perform in simulating seasonal and regional surface net radiation, latent heat and sensible heat flux; (2) whether or not surface energy balance is achieved by CMIP6 models for the past a few decades; (3) how different geographical locations and climate conditions affect the net radiation partitioning into latent heat and sensible heat. The findings of this study are expected to provide a scientific reference for regional patterns and seasonal cycles of CMIP6 models' performance in simulating surface energy flux and future model improvement.

2 Study area and data

2.1 Study area

In this study, we separate the global land surface (excluding Antarctica) into 6 major continents: Asia, Africa, Australia, Europe and Siberia, North America and Latin America (Fig. 1). These regions exhibit distinct climate conditions

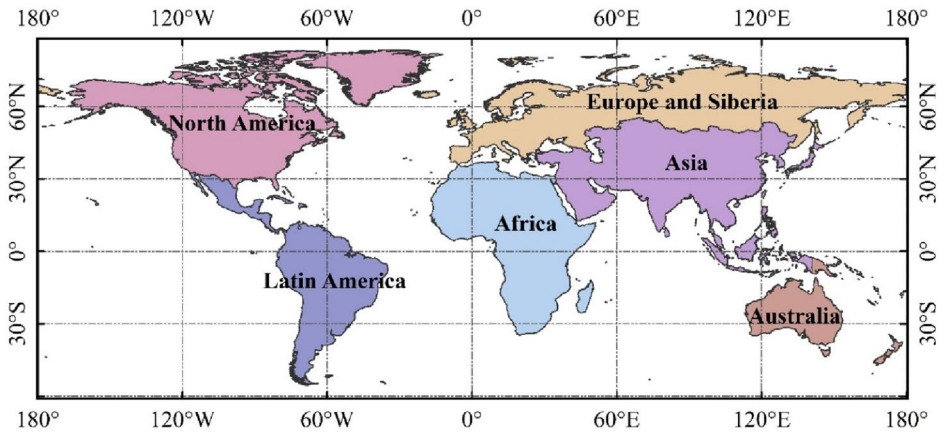

Fig. 1 Layout map of six continents analyzed in this study

and are geographically located in various latitude spans in both Northern Hemisphere and Southern Hemisphere (for instance, Europe and Siberia locate in mid-high latitudes and exhibit a moist continental and polar climate, East part of Asia locates in mid-low latitudes and has a monsoonal climate, Amazonia in South America and central part of Africa locate in low latitude and has a moist tropical climate, West part of North America and Australia locate in mid-latitude and exhibit semi-arid climate), which provide ideal test beds for investigating the spatio-temporal variations of energy balance components and their relation with geographical and climate characteristics.

2.2 Data

2.2.1 CMIP6 climate data

Monthly upwelling shortwave radiation (rsus), downwelling shortwave radiation (rsds), upwelling longwave radiation (rlus), downwelling longwave radiation (rlds), latent heat

Table 1 List of 22 CMIP6 climate models and their resolutions

Model	Institution	Country	Spatial resolution (km)	References
FGOALS-g3	Chinese Academy of Sciences	China	180 × 80	Li et al. (2020)
ACCESS-CM2	Commonwealth Scientific and Industrial Research Organisation-Australian Research Council Centre of Excellence for Climate System Science	Australia	192 × 144	Bi et al. (2020)
CESM2	National Center for Atmospheric Research	United States	288 × 192	Danabasoglu et al. (2020)
CESM2-WACCM	National Center for Atmospheric Research	United States	144 × 96	Danabasoglu et al. (2020)
CMCC-CM2-HR4	Fondazione Centro Euro-Mediterraneo sui Cambiamenti Climatici	Italy	288 × 192	Cherchi et al. (2019)
CMCC-CM2-SR5	Fondazione Centro Euro-Mediterraneo sui Cambiamenti Climatici	Italy	288 × 192	Cherchi et al. (2019)
CMCC-ESM2	Fondazione Centro Euro-Mediterraneo sui Cambiamenti Climatici	Italy	288 × 192	Lovato et al. (2022)
CNRM-ESM2-1	Centre National de Recherches Meteorologiques-Centre Europeen de Recherche et de Formation Avancee en Calcul Scientifique	France	256 × 128	Séférian et al. (2019)
MIROC-ES2L	Japan Agency for Marine-Earth Science and Technology, Atmosphere and Ocean Research Institute, National Institute for Environmental Studies, and RIKEN Center for Computational Science	Japan	128 × 64	Hajima et al. (2020)
CESM2-FV2	National Center for Atmospheric Research	United States	144 × 96	Danabasoglu et al. (2020)
CESM2-WACCM-FV2	National Center for Atmospheric Research	United States	288 × 192	Danabasoglu et al. (2020)
GFDL-ESM4	National Oceanic and Atmospheric Administration-Geophysical Fluid Dynamics Laboratory	United States	288 × 180	Dunne et al. (2020)
UKESM1-0-LL	Met Office Hadley Centre	Britain	192 × 144	Sellar et al. (2019)
IPSL-CM6A-LR	Institut Pierre Simon Laplace	France	144 × 143	Boucher et al. (2020)
CanESM5	Canadian Centre for Climate Modelling and Analysis	Canada	128 × 64	Swart et al. (2019)
MRI-ESM2-0	Meteorological Research Institute	Japan	320 × 160	Oshima et al. (2020)
BCC-CSM2-MR	Beijing Climate Center	China	320 × 160	Wu et al. (2019)
TaiESM1	Academia Sinica -Research Center for Environmental Changes	China	288 × 192	Lee et al. (2020)
MIROC6	Japan Agency for Marine-Earth Science and Technology, Atmosphere and Ocean Research Institute, National Institute for Environmental Studies, and RIKEN Center for Computational Science	Japan	256 × 128	Tatebe et al. (2019)
CAMS-CSM1-0	Chinese Academy of Meteorological Sciences	China	320 × 160	Xin-Yao et al. (2019)
ACCESS-ESM1-5	Commonwealth Scientific and Industrial Research Organisation	Australia	192 × 145	Ziehn et al. (2020)
MPI-ESM1-2-LR	Max Planck Institute for Meteorology	Germany	192 × 96	Mauritsen et al. (2019)

(hfls), sensible heat (hfss) from the most recent Coupled Model Inter-comparison Project-Phase 6 (CMIP6) are used in this study to investigate model performance in simulating energy balance and its components over global continents. We apply 22 CMIP6 model predictions (Table 1, downloaded from https://esgf-node.llnl.gov/search/cmip6/) and focus on the "historical" experiments in this study, which aims at reproducing the climate evolution of the twentieth century considering all major natural and anthropogenic forcings including changes in atmospheric greenhouse gases, aerosols and land use. Since multiple realizations of the "historical" experiments are available, the first member "ri1p1f1" (in the case of the first member does not exist, the member "ri1p1f2" is used instead) of the ensemble is used for the analysis.

2.2.2 ERA historical climate references

ERA5 is the fifth generation of atmospheric reanalysis of the global climate made by the European Centre for Medium-Range Weather Forecasts (ECMWF) based on historical observation data with the Integrated Forecasting System (IFS) model and its data assimilation system (Roussel et al. 2020). Compared with the former ERA-Interim reanalysis data, ERA5 has extended the records of atmospheric variables and land surface variables beginning from 1950 and significantly enhanced horizontal and temporal resolutions, which are 31 km and hourly respectively (Hersbach et al. 2020).

Although as a reanalysis product, ERA5 energy component data have their own biases as well, previous work has proved its suitability and applicability for being used as reference dataset. Decker et al. (2012) evaluated the reanalysis products from GMAO, NCEP, and ECMWF using FLUXNET observations, concluding that all of them overestimate the surface solar radiation with ERA data having the best accuracy. ERA data is also more suitable for European regions than JRC-MARS based on longtime series solar radiation datasets (Bojanowski et al. 2014). ERA5 downward longwave radiation is well depicted (Tang et al. 2021) compared to Clouds and Earth's Radiant Energy System (CERES) satellite retrievals and in situ observations. Overall, the reanalysis bias errors are substantially smaller than in GCM estimates, and the ERA5 dataset appears to be one of the best reanalysis products. In this study, monthly ERA5 surface net solar radiation (ssr), surface net radiation (Wielicki et al.), surface latent heat flux (slhf) and surface sensible heat (sshf) datasets (downloaded from https://cds.climate.copernicus.eu/) are used as references to evaluate CMIP6 historical prediction performance over global continents. Both the CMIP6 predictions and ERA5 reanalysis data are regridded to $1^\circ \times 1^\circ$ spatial resolution using bilinear interpolation for model comparison and performance evaluation.

3 Methodology

3.1 Assessment of CMIP6 model performance in simulating surface net radiation

3.1.1 Net radiation derivation

The net radiation flux (Rn) is the sum of the shortwave net radiation and the longwave net radiation. The shortwave net radiation is equal to the difference between the downward shortwave radiation and the upward shortwave radiation. Similarly, the longwave net radiation is equal to the difference between the downward longwave radiation and the upward longwave radiation. Thus, the net radiation can be expressed as Eq. (1):

$$Rn = Rs + Rl = R_s\downarrow - R_s\uparrow + R_l\downarrow - R_l\uparrow, \tag{1}$$

where Rs is shortwave net radiation(W/m^2), Rl is longwave net radiation; $R_s\downarrow$ and $R_s\uparrow$ are downward and upward shortwave radiation; $R_l\downarrow$, $R_l\uparrow$ refer to the downward and upward longwave radiation respectively.

3.1.2 Model performance in different seasons and regions

In this study, summer is defined as June, July, and August for the Northern Hemisphere and December, January, and February (DJF) for the Southern Hemisphere (SH). Comparatively, winter is defined as DJF for the NH and JJA for the SH. Furthermore, the global land is divided into 6 continents which are shown in Fig. 1. Specifically, we want to analyze the performance of CMIP6 models in simulating surface energy flux during different seasons and regions.

3.2 Evaluation of the components of net radiation partition

Based on surface energy balance, the vast majority of the surface net radiation is allocated to latent and sensible heat, with a small fraction allocated to soil heat flux.

$$Rn = LE + SH + G, \tag{2}$$

where LE is latent heat flux, SH is sensible heat flux, G is soil heat flux. In this study, G is assumed to be zero on the multi-year mean basis and thus can be neglected (Daughtry et al. 1990).

3.3 Performance measures

3.3.1 Model bias

The bias B is defined as the mean of monthly energy flux for each CMIP6 model divided by the mean of the corresponding ERA5 observations in each $1° \times 1°$ grid box:

$$B = \frac{\overline{Rn}_{CMIP6}}{\overline{Rn}_{ERA5}}. \quad (3)$$

3.3.2 Taylor diagrams

Taylor diagram is used to compare the relative merits of a suite of different models in this study. Taylor diagram summarizes three statistics in one figure: horizontal and vertical axes show standard deviation, the radial axis shows spatial correlation coefficient, and the concentric circle denotes centered RMSD. The values with correlation coefficient and the standard deviation are 1 and the RMSD is 0 indicate the best match between observation and model simulation. In Taylor diagram, the correlation coefficient, standard deviation and RMSD have the following relationship:

$$E'^2 = \sigma_M^2 + \sigma_r^2 - 2\sigma_M\sigma_r R, \quad (4)$$

where R is the correlation coefficient between the model and reference data. E' is the centered RMSD and σ_M^2 and σ_r^2 are the variances of the model and reference data respectively. In this study, seasonal and regional net radiation, latent heat and sensible heat climatology from CMIP6 and ERA5 references are evaluated with Taylor diagram.

3.3.3 Taylor skill score

Taylor skill score (Taylor 2001) is used to evaluate skill of the models in simulating surface energy fluxes with respect to observations:

$$T = \frac{4(1+R)}{\left(\sigma + \frac{1}{\sigma}\right)^2 (1+R_0)}, \quad (5)$$

where R is the spatial correlation coefficient between observation and model simulation, σ is the ratio of simulated to observed standard deviation, R_0 is the maximum correlation attainable that is assumed as 1. The Taylor Skill Score ranges from zero to unity, and the score equals 1 indicates a perfect simulation.

4 Results and discussion

4.1 The performance of CMIP6 models in simulating seasonal surface net radiation

The spatial patterns of bias ratio from 15 selected CMIP6 models as well as ensemble mean are shown in Fig. 2 for JJA and Fig. 3 for DJF respectively. As illustrated, overall CMIP6 models can capture the spatial pattern of Rn, the biases for most continents are within 30%. However, predictions of net radiation (Rn) from CMIP6 models show obvious differences for JJA and DJF. In general, most CMIP6 models overestimate Rn in JJA and underestimate Rn in DJF. For instance, most models overestimate Rn in JJA but underestimate Rn in DJF over Central Asia and Western Europe. The model simulation bias of Rn is larger in JJA than DJF over Amazon.

Figure 4a presents the seasonal biases of Rn, which shows slightly inter-model variability exists over different continents. Some models (such as CESM2, CESM2-WACCM, CESM2-FV2, CESM2-WACCM-FV2, IPSL-CM6A-LR) display relatively smaller biases for JJA and DJF. Comparatively, other models (such as FGOALS-g3 and MPI-ESM1-2-LR) show larger model biases. Figure 4b and d indicate that models overestimate Rn for both JJA and DJF over Africa and Australia, especially in the Saharan region and the central and western parts of Australia (as can be seen in Figs. 2 and 3). The reason that CMIP6 models overestimate Rn for these regions might be that the Saharan and central-western Australia regions are covered with deserts, and desert dust suspended in the atmosphere (generally regarded as an aerosol constituent) affect both incoming shortwave and outgoing longwave radiation, which is difficult be simulated by models (Menon et al. 2002). CMIP6 models significantly overestimate Rn in DJF and slightly overestimate Rn in JJA over Asia (Fig. 4c), especially in the Tibetan Plateau, which is probably associated with relatively coarse horizontal model resolutions which could not capture the abrupt changes in topography (Li et al. 2021). In addition, Tibetan Plateau has the largest and thickest frozen ground at the middle and low latitudes (Luo et al. 2020), hence the complexity of the freeze–thaw process reflects the considerable uncertainties inherent in climate models. Figure 4e shows larger biases exist for DJF over Europe and Siberia, which might be closely related to the presence of clouds (since there are more clouds in winter than in summer over Europe and Siberia). As pointed out in IPCC AR6, the simulation of clouds and their feedback may be still problematic in climate models, although some CMIP6 models demonstrate an improvement in how clouds are represented. The absorption of radiation in clouds may

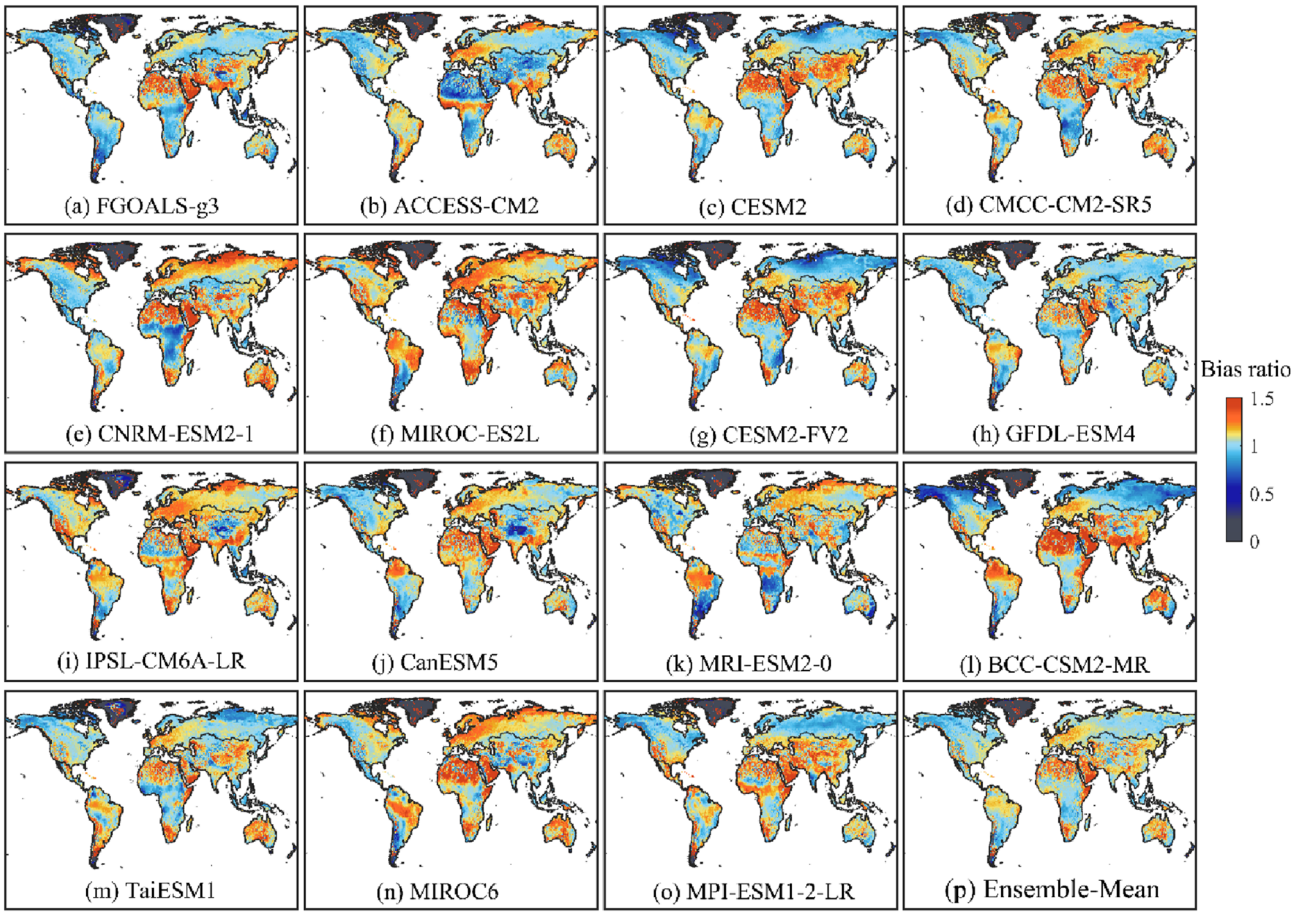

Fig. 2 Bias ratio (with optimal value = 1) of JJA net radiation from 15 models out of 22 selected climate models and ensemble mean with respect to ERA5

be considerably larger than assumed in models (Cess et al. 1995; Ramanathan et al. 1995). Furthermore, sparse observation stations lead to detection difficulty in understanding the spatial and temporal changes of clouds, which also prevents cloud simulation by models (Zajaczkowski et al. 2013). Figures 4f, 2 and 3 indicate that most models overestimate Rn over the Amazon region for JJA and DJF. Vegetation may be partly responsible for the differences in both seasons. It is well-known that the largest tropical rainforest on Earth grows in the Amazon, and vegetation influences the energy flux between land and the atmosphere (Bonan 2008). For instance, Liu et al. (2021) presented that vegetation can intercept some solar radiation, which leads to substantial differences in the amount of radiation on the top of vegetation and the ground surface below the tree canopy, generating vegetation canopy shading. However, the size of the Amazon rainforest shrank dramatically. Deforestation increases surface albedo, reduces Leaf Area Index (LAI) and canopy height, and changes emissions of CO_2, trace gases, and aerosols. Figure 4g displays the biases of CMIP6 models for North America and it shows that most models tend to underestimate Rn in JJA for Greenland (also see Fig. 2), which may be related to ice sheet melt in JJA. Melting sharply from the ice margin toward the interior decreases surface albedo and limits the emissions of outgoing longwave radiation, eventually resulting in dramatical increase in net radiation (van den Broeke et al. 2008). Besides, most models show substantial biases over the mountainous region (such as Colorado and Utah) of the United States (Fig. 3). It is difficult for the complex terrain to be accurately simulated due to relatively coarse horizontal model resolutions (Hofer et al. 2012; Ludwig et al. 2016). The topographic shading and the surrounding complex terrain can also strongly influence solar radiation.

Figures S1 and S2 present violin plots of the spatial–temporal averaged Rn biases from the 22 CMIP6 models. As shown, the biases of Rn for models are larger during DJF (ranges between 0 and 2.5) than JJA (ranges between 0 and 2), and the differences of the inter-model simulations are small, except for a slight difference during DJF in Australia as well as Europe and Siberia. The medians of some models

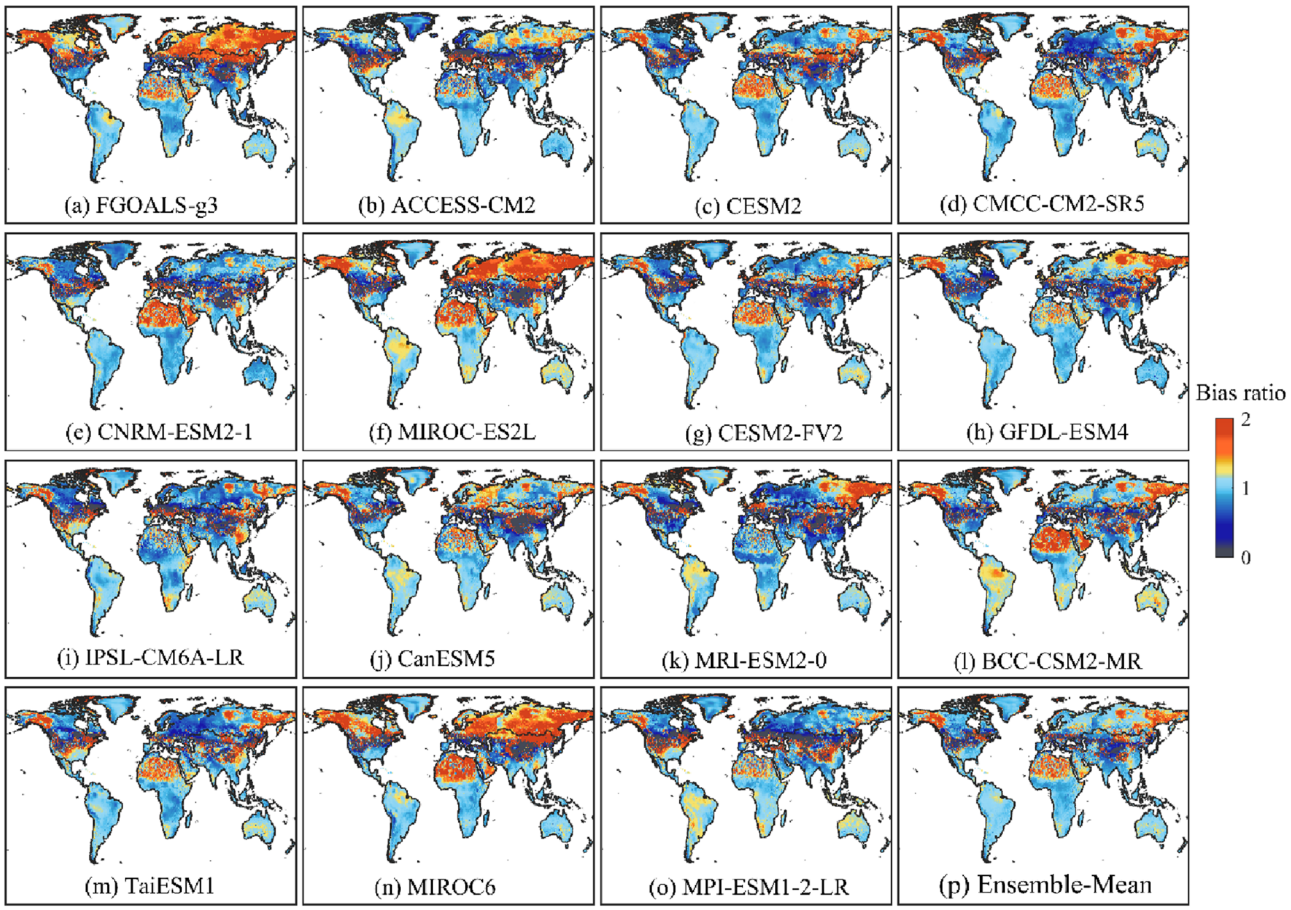

Fig. 3 Bias ratio (with optimal value = 1) of DJF net radiation from 15 models out of 22 selected climate models and ensemble mean with respect to ERA5

such as FGOALS-g3, CMCC-CM2-HR4, MIROC-ES2L, and MIROC6 are greater than 1, indicating that these models overestimate net radiation in general.

We further compare the CMIP6 model's performance of Rn prediction through the Taylor diagrams (Taylor 2001) as shown in Figs. 5 and 6. Figure 5 indicates that the distributions of models are quite concentrated for each continent in JJA. Most models have spatial correlations from 0.9 to 0.95 and the ratio of spatial standard deviations is near 1, indicating that models perform consistently well over the selected six continents in JJA. However, in contrast, model predictions show larger inconsistency to ERA5 reanalysis data in DJF, particularly in Asia, Europe and Siberia, and North America. Specifically, in Asia, the correlation coefficients of 22 models are down to 0.8 (from 0.9), and the spatial standard deviations exceed 1. In Europe and Siberia, and North America, models are more scattered in the Taylor plot. The model biases of simulating Rn in DJF are larger than JJA over Asia, Europe and Siberia, and North America, which could be associated with the bias of precipitation in DJF. Precipitation directly affects the amount of water vapor in the atmosphere, which further affects solar shortwave radiation on the ground. Most models overestimate precipitation in DJF over the western part of North America and Asia, which leads to overestimation of water vapor in the atmosphere and underestimation of solar shortwave radiation in DJF, eventually, resulting in underestimation of net radiation over North America and Asia. For Europe and Siberia, the model biases of simulating Rn in DJF (underestimate) are larger than simulations in JJA, which might be closely related to the presence of clouds, since there are more clouds in DJF than JJA over Europe and Siberia.

Besides, the Taylor skill scores are also applied to rank the performance of CMIP6 models in simulating Rn for JJA and DJF (see Fig. S3). The Rn scores ranged between 0.95 and 1 for both seasons over Global land surface, where TaiESM1 performs the best for JJA, and GFDL-ESM4 performs the best for DJF. For JJA over six continents, CMCC-CM2-HR4 outperforms other models over Africa, CMCC-ESM2 and TaiESM1 perform the best over Asia, both CNRM-ESM2-1 and CESM2-WACCM-FV2 score 0.98 over Australia, IPSL-CM6A-LR performs better than

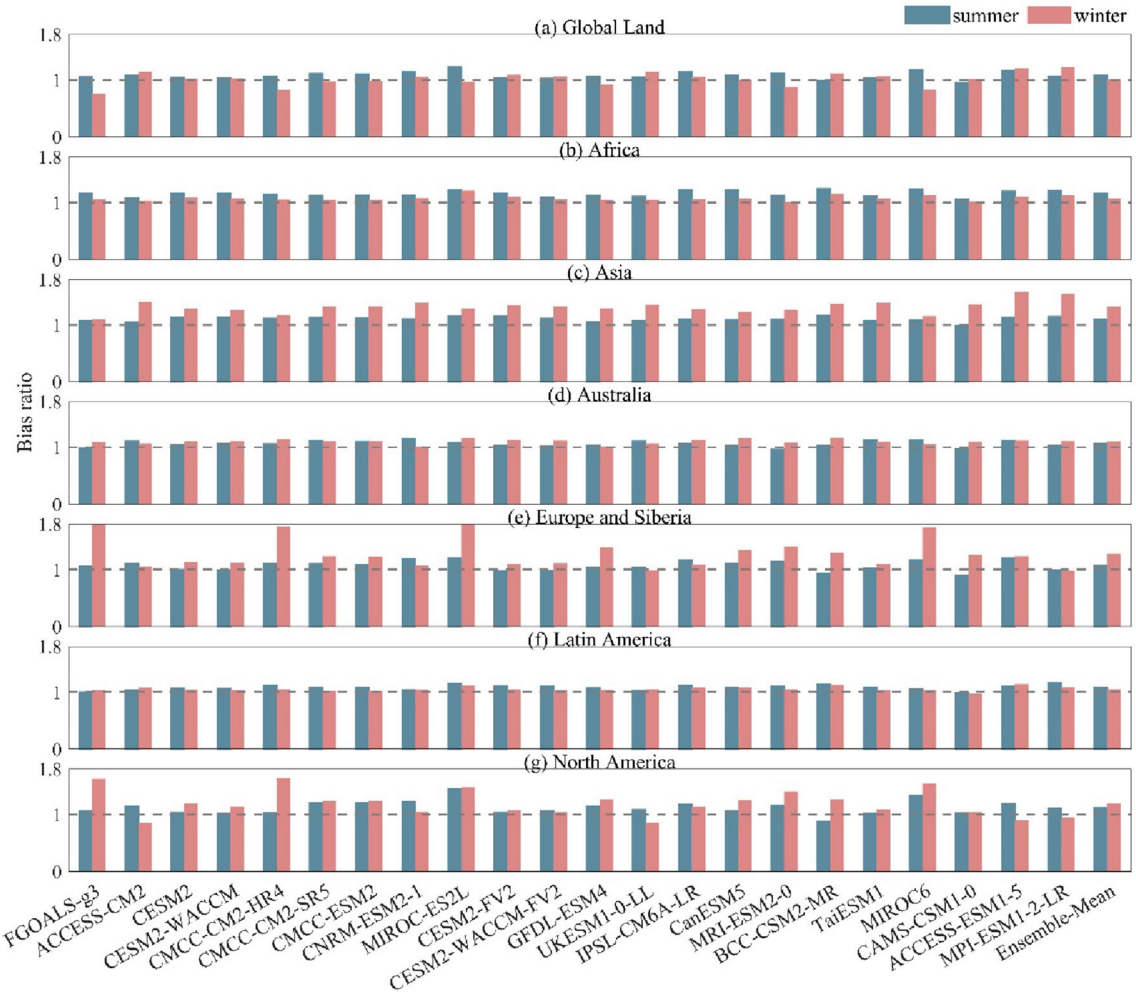

Fig. 4 Net radiation bias of CMIP6 over (**a**) Global Land, (**b**) Africa, (**c**) Asia, (**d**) Australia, (**e**) Europe, (**f**) Latin America, and (**g**) North America in JJA and DJF

others over Europe and Siberia, UKESM1-0-LL performs the best over Latin America, and ACCESS-ESM1-5 performes the best over North America. Comparatively for DJF, CMCC-CM2-HR4 shows the best score over Africa (up to 0.99), CMCC-CM2-SR5 reaches 0.98 over Asia, GFDL-ESM4 performs the best for Australia, CESM2-WACCM outperforms other models over Europe and Siberia, CNRM-ESM2-1 performs better than others over Latin America, and CESM2-WACCM performs the best for North America.

4.2 Net radiation partition and surface energy balance simulated by CMIP6 models

The surface net radiation consists of the shortwave net radiation and the longwave net radiation at the surface of Earth. It provides the vast majority of energy for the non-radiative fluxes of the surface energy balance, particularly the surface sensible heat flux and latent heat flux (Bisht et al. 2005; Wild 2020). Figures 7 and 8 summarize the partition between surface sensible heat and latent heat flux over global continents in both seasons, respectively. As shown, the percentage of LH generally is higher than SH in both seasons, however, although the models' mean SH is negative being consistent with ERA5 over Europe and Siberia, and North America, the inter-model spread is considerably large, indicating that CMIP6 models could not accurately simulate sensible heat flux for DJF.

4.3 Seasonal characteristics of model biases in simulating latent heat and sensible heat over different continents

To further quantify the model performance of simulated non-radiative fluxes, the LH biases and SH biases relative to ERA5 are shown in Fig. 9. Models show obvious differences in simulating LH and SH over different continents. For LH, the simulated winter LH biases are higher than that of

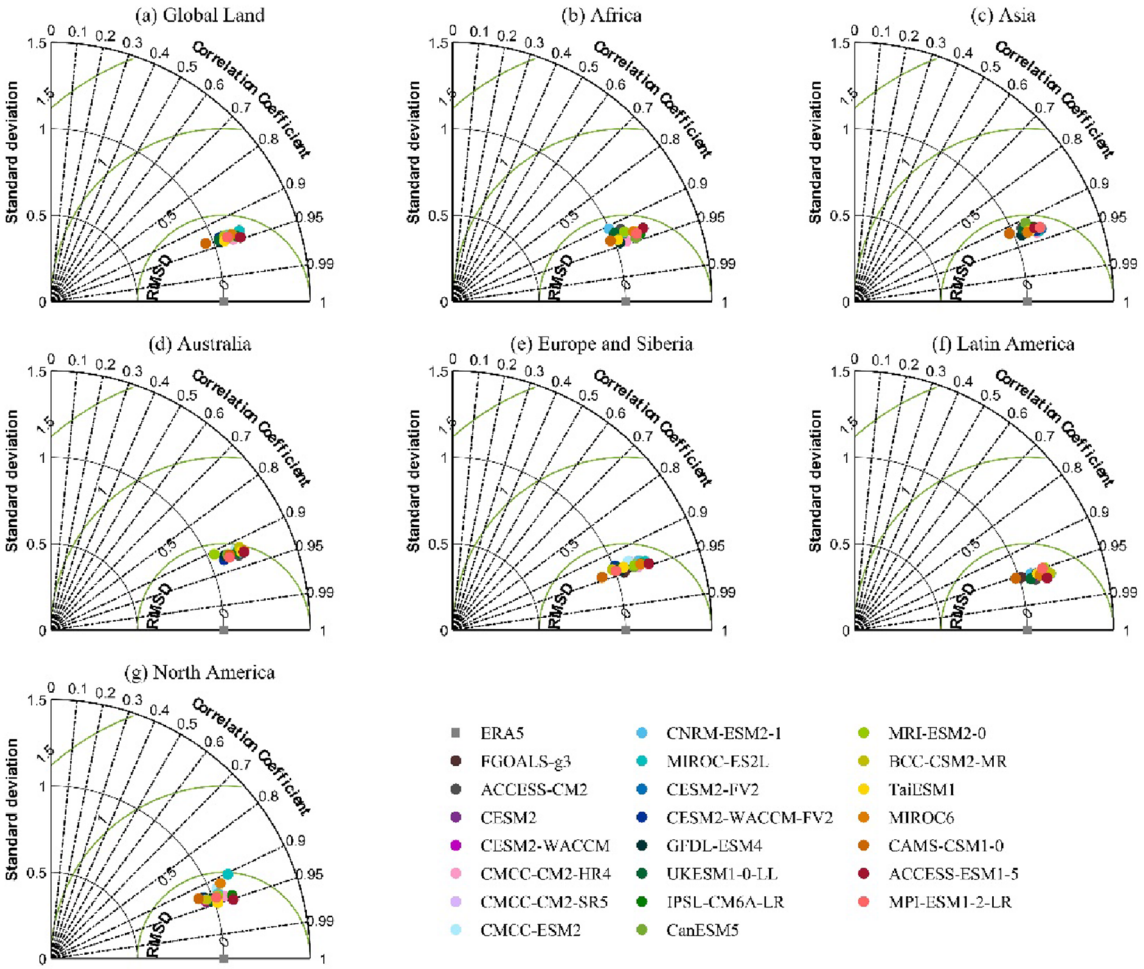

Fig. 5 Taylor diagrams of JJA net radiation simulation over global continents. The radial coordinate is the magnitude of the standard deviation (denoted by black arcs). The concentric green semi-circles denote root-mean-square difference values. The angular coordinate shows the correlation coefficient (denoted by dotted black lines)

summer. Models generally overestimate winter LH for Australia, Europe and Siberia, and Latin America (The winter months in Australia are June, July and August), however, it is noteworthy that summer LH simulations near-perfect match the reference value. The LH biases of CMIP6 models are principally caused by precipitation and surface soil moisture. On the one hand, the overestimation of precipitation by the CMIP6 models possibly caused considerable uncertainties in simulating the LH (Almazroui et al. 2020; Han et al. 2017). On the other hand, the effects of vegetation include transpiration, canopy interception of rainfall, and root interception tend to affect soil moisture (Williams and Torn 2015). Additionally, the uncertainties of satellite land cover products also impact the accuracy of global terrestrial latent heat simulations (Yao et al. 2016).

For SH, the variation of biases is substantial during DJF over different continents, although there is remarkable agreement between the model and the ERA5 reanalysis data during JJA. As shown, models showing negative biases during DJF (over Europe and Siberia), such as CESM2-FV2 and CESM2-WACCM-FV2. A few studies showed that cloudiness plays an important role in surface SH through its influence on radiation flux and soil temperature (Zhou and Du 2016). Furthermore, both topographic shading and vegetation canopy shading that changes with solar altitude angle can reduce sensible heat flux (Liu et al. 2022a, b; Marsh et al. 2012; Zhang et al. 2020). Besides, the sensible heat biases of CMIP6 models are also largely impacted by wind speed (Yang et al. 2011).

In addition, we rank the Taylor skill scores of LH and SH simulations and the results are shown in Figure S4. As for LH, CMCC-CM2-HR4 performs the best for JJA and GFDL-ESM4 performs the best for DJF over Global Land. In Africa, CESM2-WACCM, CMCC-CM2-HR4, and TaiESM1 score 0.97 for JJA, GFDL-ESM4 scores 0.98 for DJF. In Asia, CMCC-CM2-HR4 outperforms other

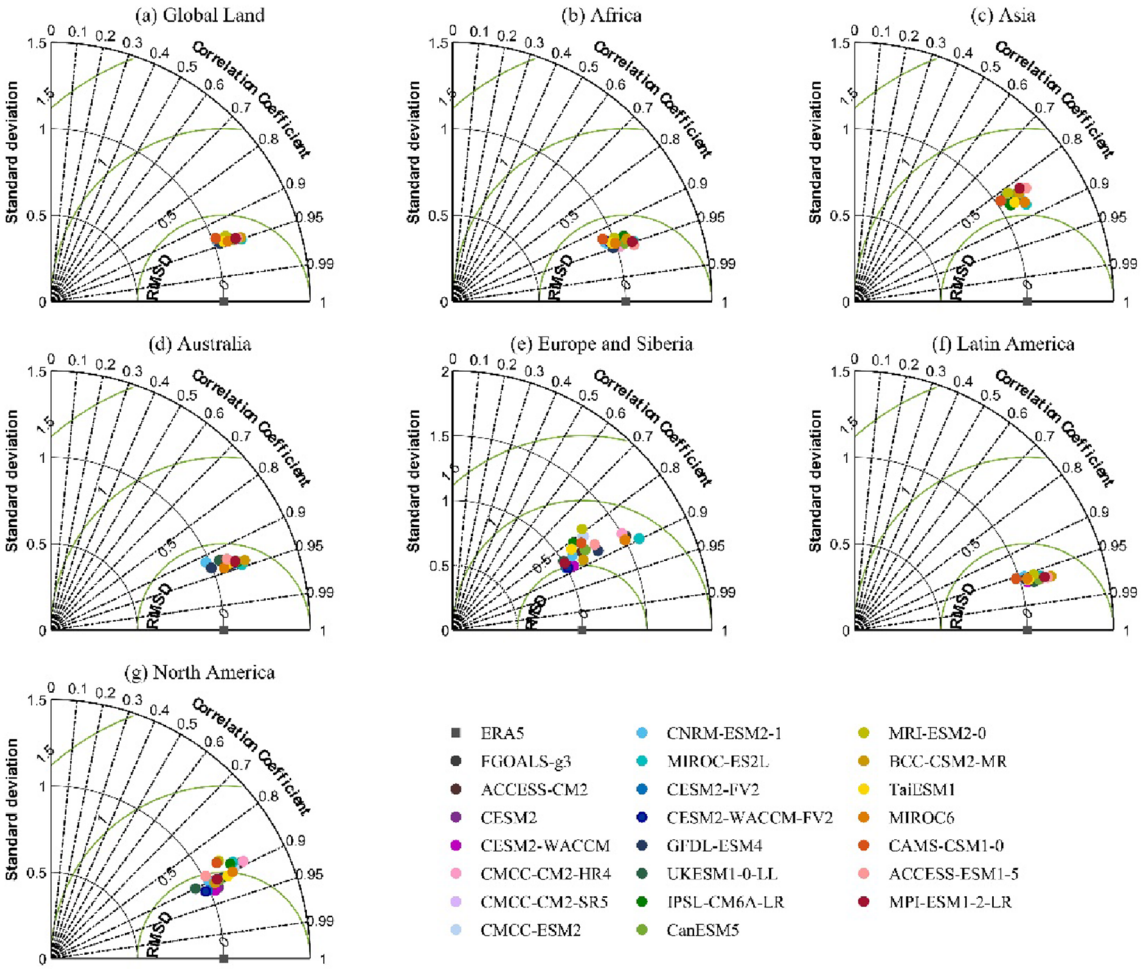

Fig. 6 Taylor diagrams of DJF net radiation simulation over global continents. The radial coordinate is the magnitude of the standard deviation (denoted by black arcs). The concentric green semi-circles denote root-mean-square difference values. The angular coordinate shows the correlation coefficient (denoted by dotted black lines)

models for JJA, and CAMS-CSM1-0 performs the best for DJF. MIROC6 shows the highest Taylor skill score (0.63) for JJA, and GFDL-ESM4 shows a better score (0.97) for DJF over Australia. For Europe and Siberia, CMCC-CM2-SR5 is the best model in JJA, CAMS-CSM1-0 is optimal in DJF. It's noteworthy that the CMIP6 models perform worse in these two regions with the scores decreasing from 0.6 to 0.3 over Australia in JJA and from 0.5 to 0.3 over Europe and Siberia in DJF. In Latin America and North America, CESM2 and ACCESS-CM2 behave the best in JJA and ACCESS-CM2 and GFDL-ESM4 perform the best for DJF.

As for SH, the highest Taylor skill score for JJA is obtained by CESM2 (over Global Land and over North America), IPSL-CM6A-LR (over Africa), CESM2-WACCM (over Asia), CMCC-CM2-HR4 (over Australis), CMCC-CM2-SR5 (over Europe and Siberia), ACCESS-ESM1-5 (over Latin America) respectively. In comparison, the highest Taylor skill score for DJF is obtained by CESM2 (over Global Land, Asia, Australia), CESM2-WACCM-FV2 (over Africa), MIROC6 (Europe and Siberia), CESM2-WACCM (Latin America), CMCC-ESM2 (North America) respectively.

Global warming could affect surface energy fluxes. The increase of carbon dioxide also yields a nearly steady increase of the downward longwave radiation at the surface (Hu et al. 2019), this further affects the partition of net radiation and its components. Global warming also increases the ability to evaporate (in form of latent heat).

5 Conclusions

In this study, we evaluated the performance of 22 CMIP6 models in simulating seasonal surface energy flux during 1950–2014 over global land surface as well as six continents,

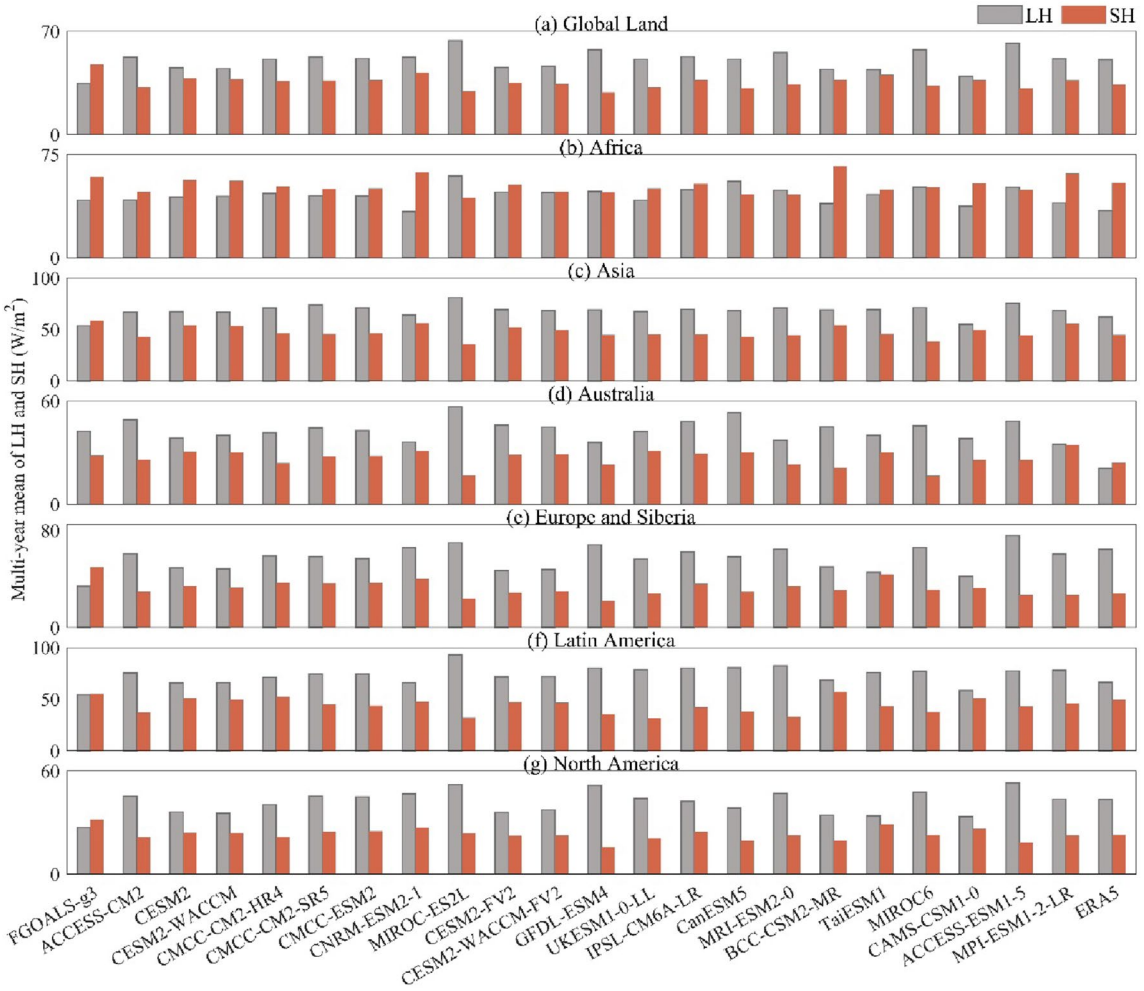

Fig. 7 Partition of latent heat and sensible heat over global continents during JJA (W/m^2), the last one is ERA5 reference

and analyzed net radiation partition and surface energy balance simulated by CMIP6 models. The main conclusions are summarized as follows:

1. Simulations of net radiation (Rn) show obvious seasonality over global land surface. In general, net radiation simulations match better with ERA5 reference data in JJA than DJF, but the biases are within 30% for both seasons. The CMIP6 models slightly overestimate net radiation in JJA and underestimate net radiation in DJF.
2. Models substantially overestimate Rn over Africa, Australia, and Latin America, especially in the Saharan and Tibetan Plateau, which is probably associated with land topography. The model bias of Rn is larger in DJF than JJA over Asia, Europe and Siberia, and North America.
3. As for the non-radiative fluxes, the percentage of LH in Rn is higher than SH. The bias of simulated LH in DJF (near 30%) is higher than JJA. In addition, LH predictions vary significantly among different continents: models overestimate LH over Australia, Europe and Siberia, and Latin America in DJF whereas LH perform near-perfect match with the reference value (biases values are around 1) in JJA.
4. Contrary to ERA5, the mean prediction of SH by CMIP6 models is positive during DJF (except for Europe and Siberia, and North America), and the inter-model variability is substantial over different continents. Moreover, despite models' mean SH is negative, which is consistent with ERA5 over Europe and Siberia, and North America, the inter-model spread is remarkably large. There-

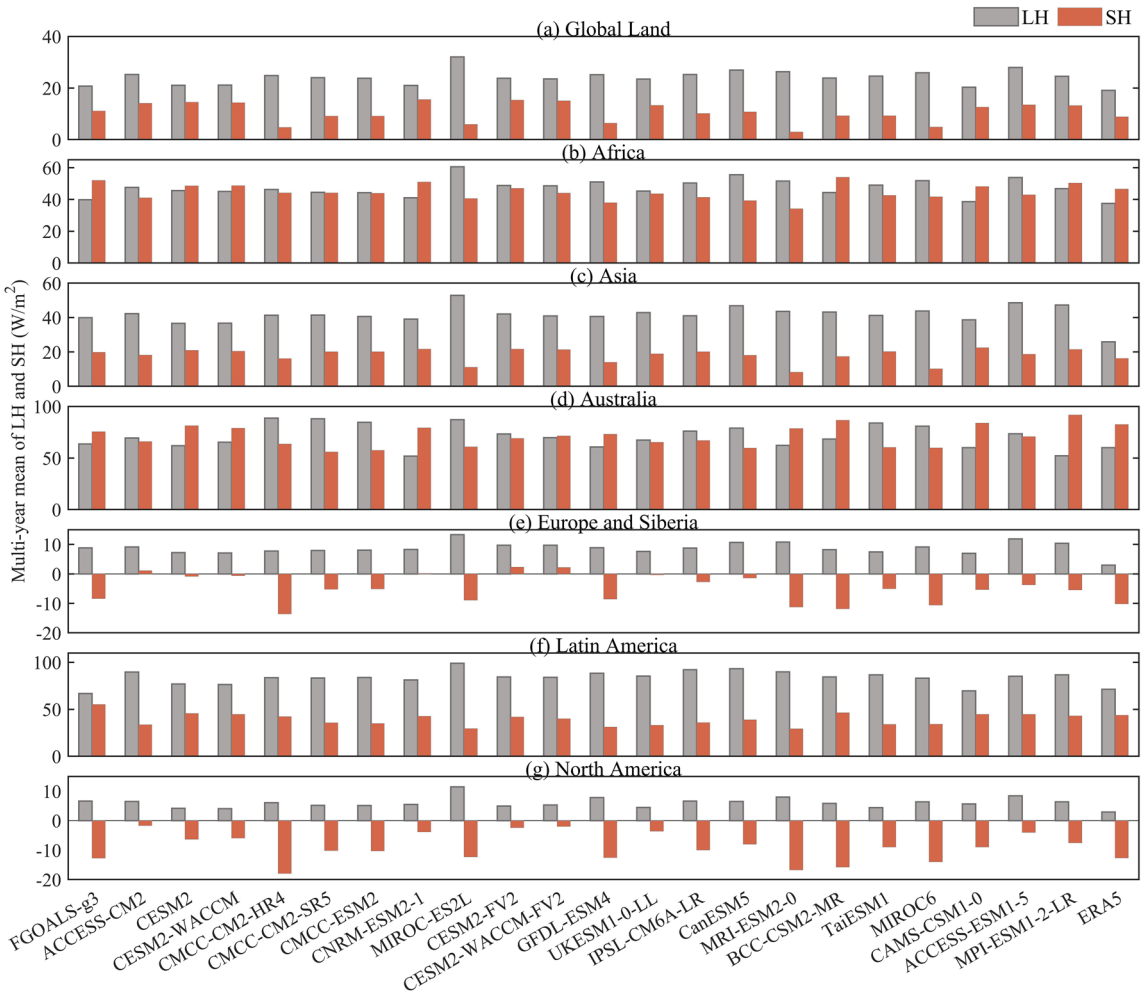

Fig. 8 Partition of latent heat and sensible heat over global continents during DJF (W/m^2), the last one is ERA5 reference

fore, the biases of SH are substantial during DJF over different continents and models significantly underestimate SH (the bias ratios of some models are even less than negative 1), indicating that current CMIP6 models could not accurately capture sensible heat flux for DJF.

5. The performance of CMIP6 in Rn simulation (Taylor skill score ranged between 0.85 and 1) is better than LH and SH simulations (Taylor skill score ranged between 0.3 and 1) for JJA and DJF. As for JJA, TaiESM1 performs the best for Rn simulations, CMCC-CM2-HR4 is the best model in simulating LH and CESM2 outperforms other models in simulating SH. Comparatively, GFDL-ESM4 performs the best in Rn and LH simulations and CESM2 outperforms other models in simulating SH in DJF.
6. Climate change marked by fast and continuous global warming is influenced by the greenhouse gases in air, and the increase of carbon dioxide yields nearly steady increase of the downward longwave radiation at the surface. This further affects the partition of net radiation and its components. Therefore, assessing the prediction accuracy of surface energy balance components is very crucial for understanding the impact of global warming and provide references for future model development. Although the emphasis of this paper is placed on the performance and variations in surface energy fluxes for historical data since the reference exist in this period, it is also essential to work on investigating the variation of energy fluxes for future projections, which we intend to conduct analysis in our future work.

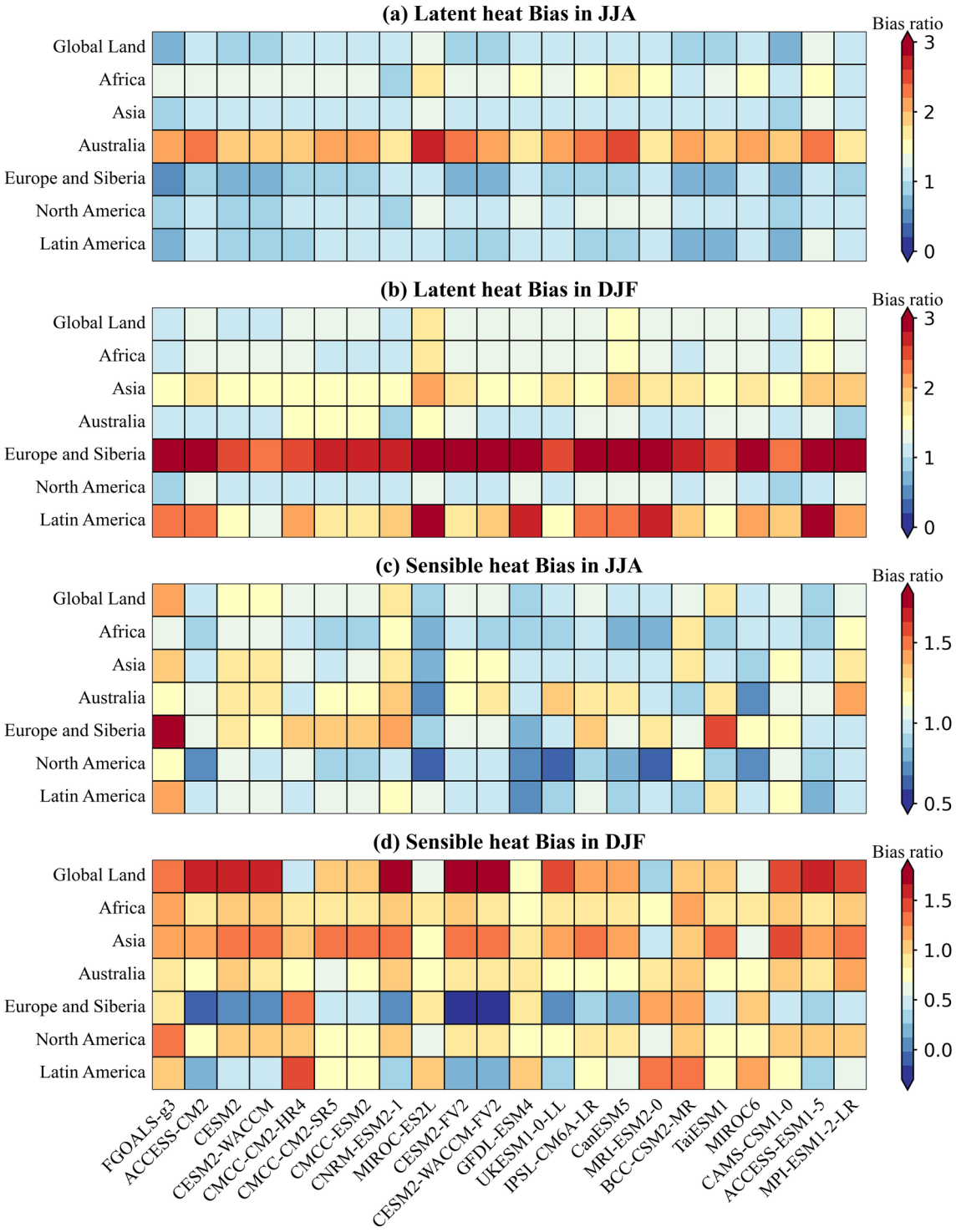

Fig. 9 Heatmaps of multi-year (1950–2014) mean CMIP6 model biases for LH, SH over global continents

Supplementary Information The online version contains supplementary material available at https://doi.org/10.1007/s00382-022-06595-5.

Acknowledgements The authors acknowledge the World Climate Research Program for managing and providing CMIP6 data.

Author contributions SL and ZL are co-first authors and contribute equally to the manuscript. SL: methodology, data acquisition, software, writing-original draft. ZL: conceptualization, methodology, writing-original draft, funding acquisition, supervision. QD: funding acquisition, editing, supervision. BH: data acquisition, editing.

Funding This work is supported by the National Key Research and Development Program of China (#2021YFC3201100), Natural Science Foundation of Jiangsu Province (#BK20220992), Fundamental Research Funds for the Central Universities (#B220201027), Strategic Priority Research Program of the Chinese Academy of Sciences (#XDA20060401) and High level introduction of talent research start-up fund of Hohai University (#522020012).

Data availability The authors state that the data of this study can be shared based on reasonable request. CMIP6 data can be downloaded from https://esgf-node.llnl.gov/search/cmip6/. ERA5 reanalysis data can be downloaded from https://cds.climate.copernicus.eu/.

Declarations

Conflict of interest The authors declare that no known competing financial interests to influence this study.

Ethical approval The authors consent that there exist none ethical issues in this manuscript.

Consent to participate All authors agree to the materials submitted and consent to their participation.

References

AghaKouchak A, Mehran A (2013) Extended contingency table: performance metrics for satellite observations and climate model simulations. Water Resour Res 49:7144–7149. https://doi.org/10.1002/wrcr.20498

Almazroui M, Saeed S, Saeed F, Islam MN, Ismail M (2020) Projections of precipitation and temperature over the South Asian countries in CMIP6. Earth Syst Environ 4:297–320. https://doi.org/10.1007/s41748-020-00157-7

Bi D, Dix M, Marsland S, O'farrell S, Sullivan A, Bodman R, Law R, Harman I, Srbinovsky J, Rashid HA (2020) Configuration and spin-up of ACCESS-CM2, the new generation Australian community climate and earth system simulator coupled model. J South Hemisphere Earth Syst Sci 70:225–251. https://doi.org/10.1071/ES19040

Bisht G, Venturini V, Islam S, Jiang L (2005) Estimation of the net radiation using MODIS (moderate resolution imaging spectroradiometer) data for clear sky days. Remote Sens Environ 97:52–67. https://doi.org/10.1016/j.rse.2005.03.014

Bojanowski JS, Vrieling A, Skidmore AK (2014) A comparison of data sources for creating a long-term time series of daily gridded solar radiation for Europe. Sol Energy 99:152–171. https://doi.org/10.1016/j.solener.2013.11.007

Bonan GB (2008) Forests and climate change: forcings, feedbacks, and the climate benefits of forests. Science 320:1444–1449. https://doi.org/10.1126/science.1155121

Boucher O, Servonnat J, Albright AL, Aumont O, Balkanski Y, Bastrikov V, Bekki S, Bonnet R, Bony S, Bopp L (2020) Presentation and evaluation of the IPSL-CM6A-LR climate model. J Adv Model Earth Syst. https://doi.org/10.1029/2019MS002010

Ceppi P, Gregory JM (2019) A refined model for the Earth's global energy balance. Clim Dyn 53:4781–4797. https://doi.org/10.1007/s00382-019-04825-x

Cess RD, Zhang M, Minnis P, Corsetti L, Dutton E, Forgan B, Garber D, Gates W, Hack J, Harrison E (1995) Absorption of solar radiation by clouds: observations versus models. Science 267:496–499. https://doi.org/10.1126/science.267.5197.496

Cherchi A, Fogli PG, Lovato T, Peano D, Iovino D, Gualdi S, Masina S, Scoccimarro E, Materia S, Bellucci A (2019) Global mean climate and main patterns of variability in the CMCC-CM2 coupled model. J Adv Model Earth Syst 11:185–209. https://doi.org/10.1029/2018MS001369

Conte L, Renner M, Brando P, Oliveira dos Santos C, Silvério D, Kolle O, Trumbore SE, Kleidon A (2019) Effects of tropical deforestation on surface energy balance partitioning in southeastern Amazonia estimated from maximum convective power. Geophys Res Lett 46:4396–4403. https://doi.org/10.1029/2018GL081625

Danabasoglu G, Lamarque JF, Bacmeister J, Bailey D, DuVivier A, Edwards J, Emmons L, Fasullo J, Garcia R, Gettelman A (2020) The community earth system model version 2 (CESM2). J Adv Model Earth Syst. https://doi.org/10.1029/2019MS001916

Daughtry C, Kustas WP, Moran M, Pinter P Jr, Jackson R, Brown P, Nichols W, Gay L (1990) Spectral estimates of net radiation and soil heat flux. Remote Sens Environ 32:111–124. https://doi.org/10.1016/0034-4257(90)90012-B

Decker M, Brunke MA, Wang Z, Sakaguchi K, Zeng X, Bosilovich MG (2012) Evaluation of the reanalysis products from GSFC, NCEP, and ECMWF using flux tower observations. J Clim 25:1916–1944. https://doi.org/10.1175/JCLI-D-11-00004.1

Dickinson RE (1995) Land-atmosphere interaction. Rev Geophys 33:917–922. https://doi.org/10.1029/95RG00284

Dunne J, Horowitz L, Adcroft A, Ginoux P, Held I, John J, Krasting J, Malyshev S, Naik V, Paulot F (2020) The GFDL earth system model version 4.1 (GFDL-ESM 4.1): overall coupled model description and simulation characteristics. J Adv Model Earth Syst. https://doi.org/10.1029/2019MS002015

Eyring V, Bony S, Meehl GA, Senior CA, Stevens B, Stouffer RJ, Taylor KE (2016) Overview of the coupled model intercomparison project phase 6 (CMIP6) experimental design and organization. Geosci Model Develop 9:1937–1958. https://doi.org/10.5194/gmd-9-1937-2016

Hajima T, Watanabe M, Yamamoto A, Tatebe H, Noguchi MA, Abe M, Ohgaito R, Ito A, Yamazaki D, Okajima H (2020) Development of the MIROC-ES2L Earth system model and the evaluation of biogeochemical processes and feedbacks. Geosci Model Develop 13:2197–2244. https://doi.org/10.5194/gmd-13-2197-2020

Han C, Ma Y, Chen X, Su Z (2017) Trends of land surface heat fluxes on the Tibetan Plateau from 2001 to 2012. Int J Climatol 37:4757–4767. https://doi.org/10.1002/joc.5119

Hersbach H, Bell B, Berrisford P, Hirahara S, Horányi A, Muñoz-Sabater J, Nicolas J, Peubey C, Radu R, Schepers D (2020) The ERA5 global reanalysis. Q J R Meteorol Soc 146:1999–2049. https://doi.org/10.1002/qj.3803

Hirschi M, Seneviratne SI, Alexandrov V, Boberg F, Boroneant C, Christensen OB, Formayer H, Orlowsky B, Stepanek P (2011) Observational evidence for soil-moisture impact on hot extremes in southeastern Europe. Nat Geosci 4:17–21. https://doi.org/10.1038/ngeo1032

Hofer D, Raible C, Dehnert A, Kuhlemann J (2012) The impact of different glacial boundary conditions on atmospheric dynamics and precipitation in the North Atlantic region. Clim Past 8:935–949. https://doi.org/10.5194/cp-8-935-2012

Hu X, Sejas SA, Cai M, Taylor PC, Deng Y, Yang S (2019) Decadal evolution of the surface energy budget during the fast warming and global warming hiatus periods in the ERA-interim. Clim Dyn 52:2005–2016. https://doi.org/10.1007/s00382-018-4232-1

Huber M, Knutti R (2012) Anthropogenic and natural warming inferred from changes in Earth's energy balance. Nat Geosci 5:31–36. https://doi.org/10.1038/ngeo1327

Kato S, Rose FG, Rutan DA, Thorsen TJ, Loeb NG, Doelling DR, Huang X, Smith WL, Su W, Ham S-H (2018) Surface irradiances of edition 40 clouds and the earth's radiant energy system

(CERES) energy balanced and filled (EBAF) data product. J Clim 31:4501–4527. https://doi.org/10.1175/JCLI-D-17-0523.1

Lee W-L, Wang Y-C, Shiu C-J, Tsai I-c, Tu C-Y, Lan Y-Y, Chen J-P, Pan H-L, Hsu H-H (2020) Taiwan Earth system model version 1: description and evaluation of mean state. Geosci Model Develop 13:3887–3904. https://doi.org/10.5194/gmd-13-3887-2020

Li L, Yu Y, Tang Y, Lin P, Xie J, Song M, Dong L, Zhou T, Liu L, Wang L (2020) The flexible global ocean-atmosphere-land system model grid-point version 3 (FGOALS-g3): description and evaluation. J Adv Model Earth Syst. https://doi.org/10.1029/2019MS002012

Li J, Miao C, Wei W, Zhang G, Hua L, Chen Y, Wang X (2021) Evaluation of CMIP6 global climate models for simulating land surface energy and water fluxes during 1979–2014. J Adv Model Earth Syst. https://doi.org/10.1029/2021MS002515

Liu Z, Merwade V (2018) Accounting for model structure, parameter and input forcing uncertainty in flood inundation modeling using Bayesian model averaging. J Hydrol 565:138–149. https://doi.org/10.1016/j.jhydrol.2018.08.009

Liu Z, Merwade V (2019) Separation and prioritization of uncertainty sources in a raster based flood inundation model using hierarchical Bayesian model averaging. J Hydrol 578:124100. https://doi.org/10.1016/j.jhydrol.2019.124100

Liu Z, Mehran A, Phillips TJ, AghaKouchak A (2014) Seasonal and regional biases in CMIP5 precipitation simulations. Climate Res 60:35–50. https://doi.org/10.3354/cr01221

Liu Z, Herman JD, Huang G, Kadir T, Dahlke HE (2021) Identifying climate change impacts on surface water supply in the southern Central Valley. Calif Sci Total Environ 759:143429. https://doi.org/10.1016/j.scitotenv.2020.143429

Liu W, Guan H, Gutiérrez-Jurado HA, Banks EW, He X, Zhang X (2022a) Modelling quasi-three-dimensional distribution of solar irradiance on complex terrain. Environ Model Softw 149:105293. https://doi.org/10.1016/j.envsoft.2021.105293

Liu Z, Duan Q, Fan X, Li W, Yin J (2022b) Bayesian retro-and prospective assessment of CMIP6 climatology in pan third pole region. Clim Dyn. https://doi.org/10.1007/s00382-022-06345-7

Loeb NG, Doelling DR, Wang H, Su W, Nguyen C, Corbett JG, Liang L, Mitrescu C, Rose FG, Kato S (2018) Clouds and the earth's radiant energy system (CERES) energy balanced and filled (EBAF) top-of-atmosphere (TOA) edition-4.0 data product. J Clim 31:895–918. https://doi.org/10.1175/JCLI-D-17-0208.1

Lovato T, Peano D, Butenschön M, Materia S, Iovino D, Scoccimarro E, Fogli P, Cherchi A, Bellucci A, Gualdi S (2022) CMIP6 simulations with the CMCC Earth system model (CMCC-ESM2). J Adv Model Earth Syst. https://doi.org/10.1029/2021MS002814

Ludwig P, Schaffernicht EJ, Shao Y, Pinto JG (2016) Regional atmospheric circulation over Europe during the Last Glacial maximum and its links to precipitation. J Geophys Res 121:2130–2145. https://doi.org/10.1002/2015JD024444

Luo S, Wang J, Pomeroy JW, Lyu S (2020) Freeze–thaw changes of seasonally frozen ground on the Tibetan Plateau from 1960 to 2014. J Clim 33:9427–9446. https://doi.org/10.1175/JCLI-D-19-0923.1

Marsh CB, Pomeroy JW, Spiteri RJ (2012) Implications of mountain shading on calculating energy for snowmelt using unstructured triangular meshes. Hydrol Process 26:1767–1778. https://doi.org/10.1002/hyp.9329

Martens B, Schumacher DL, Wouters H, Muñoz-Sabater J, Verhoest NE, Miralles DG (2020) Evaluating the land-surface energy partitioning in ERA5. Geosci Model Develop 13:4159–4181. https://doi.org/10.5194/gmd-13-4159-2020

Mauder M, Foken T, Cuxart J (2020) Surface-energy-balance closure over land: a review. Bound-Layer Meteorol 177:395–426. https://doi.org/10.1007/s10546-020-00529-6

Mauritsen T, Bader J, Becker T, Behrens J, Bittner M, Brokopf R, Brovkin V, Claussen M, Crueger T, Esch M (2019) Developments in the MPI-M Earth system model version 1.2 (MPI-ESM1. 2) and its response to increasing CO_2. J Adv Model Earth Syst 11:998–1038. https://doi.org/10.1029/2018MS001400

Menon S, Genio ADD, Koch D, Tselioudis G (2002) GCM simulations of the aerosol indirect effect: sensitivity to cloud parameterization and aerosol burden. J Atmos Sci 59:692–713

Miralles DG, Teuling AJ, Van Heerwaarden CC, Vilà-Guerau de Arellano J (2014) Mega-heatwave temperatures due to combined soil desiccation and atmospheric heat accumulation. Nat Geosci 7:345–349. https://doi.org/10.1038/ngeo2141

Oshima N, Yukimoto S, Deushi M, Koshiro T, Kawai H, Tanaka TY, Yoshida K (2020) Global and Arctic effective radiative forcing of anthropogenic gases and aerosols in MRI-ESM2. 0. Prog Earth Planet Sci 7:1–21. https://doi.org/10.1186/s40645-020-00348-w

Pendergrass AG (2020) The global-mean precipitation response to CO_2-induced warming in CMIP6 models. Geophys Res Lett. https://doi.org/10.1029/2020GL089964

Ramanathan V, Subasilar B, Zhang G, Conant W, Cess R, Kiehi J, Grassi H, Shi L (1995) Warm pool heat budget and shortwave cloud forcing: a missing physics? Science 267:499–503. https://doi.org/10.1126/science.267.5197.499

Roussel M-L, Lemonnier F, Genthon C, Krinner G (2020) Brief communication: evaluating Antarctic precipitation in ERA5 and CMIP6 against CloudSat observations. Cryosphere 14:2715–2727. https://doi.org/10.5194/tc-14-2715-2020

Séférian R, Nabat P, Michou M, Saint-Martin D, Voldoire A, Colin J, Decharme B, Delire C, Berthet S, Chevallier M (2019) Evaluation of CNRM earth system model, CNRM-ESM2-1: role of Earth system processes in present-day and future climate. J Adv Model Earth Syst 11:4182–4227. https://doi.org/10.1029/2019MS001791

Sellar AA, Jones CG, Mulcahy JP, Tang Y, Yool A, Wiltshire A, O'connor FM, Stringer M, Hill R, Palmieri J (2019) UKESM1: description and evaluation of the UK Earth system model. J Adv Model Earth Syst 11:4513–4558. https://doi.org/10.1029/2019MS001739

Shu Q, Wang Q, Song Z, Qiao F, Zhao J, Chu M, Li X (2020) Assessment of sea ice extent in CMIP6 with comparison to observations and CMIP5. Geophys Res Lett. https://doi.org/10.1029/2020GL087965

Stephens GL, Li J, Wild M, Clayson CA, Loeb N, Kato S, L'ecuyer T, Stackhouse PW, Lebsock M, Andrews T (2012) An update on Earth's energy balance in light of the latest global observations. Nat Geosci 5:691–696. https://doi.org/10.1038/ngeo1580

Swart NC, Cole JN, Kharin VV, Lazare M, Scinocca JF, Gillett NP, Anstey J, Arora V, Christian JR, Hanna S (2019) The Canadian earth system model version 5 (CanESM5. 0.3). Geosci Model Develop 12:4823–4873. https://doi.org/10.5194/gmd-12-4823-2019

Tang W, Qin J, Yang K, Zhu F, Zhou X (2021) Does ERA5 outperform satellite products in estimating atmospheric downward longwave radiation at the surface? Atmos Res 252:105453. https://doi.org/10.1016/j.atmosres.2021.105453

Tatebe H, Ogura T, Nitta T, Komuro Y, Ogochi K, Takemura T, Sudo K, Sekiguchi M, Abe M, Saito F (2019) Description and basic evaluation of simulated mean state, internal variability, and climate sensitivity in MIROC6. Geosci Model Develop 12:2727–2765. https://doi.org/10.5194/gmd-12-2727-2019

Taylor KE (2001) Summarizing multiple aspects of model performance in a single diagram. J Geophys Res 106:7183–7192. https://doi.org/10.1029/2000JD900719

Tian B, Dong X (2020) The double-ITCZ bias in CMIP3, CMIP5, and CMIP6 models based on annual mean precipitation. Geophys Res Lett. https://doi.org/10.1029/2020GL087232

Trenberth KE, Fasullo JT (2013a) An apparent hiatus in global warming? Earth's Fut 1:19–32. https://doi.org/10.1002/2013EF000165
Trenberth KE, Fasullo JT (2013b) Regional energy and water cycles: transports from ocean to land. J Clim 26:7837–7851. https://doi.org/10.1175/JCLI-D-13-00008.1
Trenberth KE, Fasullo JT, Kiehl J (2009) Earth's global energy budget. Bull Am Meteor Soc 90:311–324. https://doi.org/10.1175/2008BAMS2634.1
Trenberth KE, Zhang Y, Fasullo JT, Taguchi S (2015) Climate variability and relationships between top-of-atmosphere radiation and temperatures on Earth. J Geophys Res 120:3642–3659. https://doi.org/10.1002/2014JD022887
Ukkola A, Pitman A, Donat M, De Kauwe M, Angélil O (2018) Evaluating the contribution of land-atmosphere coupling to heat extremes in CMIP5 models. Geophys Res Lett 45:9003–9012. https://doi.org/10.1029/2018GL079102
Ukkola AM, De Kauwe MG, Roderick ML, Abramowitz G, Pitman AJ (2020) Robust future changes in meteorological drought in CMIP6 projections despite uncertainty in precipitation. Geophys Res Lett. https://doi.org/10.1029/2020GL087820
van den Broeke M, Smeets P, Ettema J, Munneke PK (2008) Surface radiation balance in the ablation zone of the west Greenland ice sheet. J Geophys Res. https://doi.org/10.1029/2007JD009283
Wang W, Chakraborty T, Xiao W, Lee X (2021) Ocean surface energy balance allows a constraint on the sensitivity of precipitation to global warming. Nat Commun 12:1–9. https://doi.org/10.1038/s41467-021-22406-7
Wielicki BA, Barkstrom BR, Harrison EF, Lee RB III, Smith GL, Cooper JE (1996) Clouds and the Earth's radiant energy system (CERES): an earth observing system experiment. Bull Am Meteor Soc 77:853–868
Wild M (2020) The global energy balance as represented in CMIP6 climate models. Clim Dyn 55:553–577. https://doi.org/10.1007/s00382-020-05282-7
Wild M, Folini D, Schär C, Loeb N, Dutton EG, König-Langlo G (2013) The global energy balance from a surface perspective. Clim Dyn 40:3107–3134. https://doi.org/10.1007/s00382-012-1569-8
Williams IN, Torn MS (2015) Vegetation controls on surface heat flux partitioning, and land-atmosphere coupling. Geophys Res Lett 42:9416–9424. https://doi.org/10.1002/2015GL066305
Wu T, Lu Y, Fang Y, Xin X, Li L, Li W, Jie W, Zhang J, Liu Y, Zhang L (2019) The Beijing climate center climate system model (BCC-CSM): the main progress from CMIP5 to CMIP6. Geosci Model Develop 12:1573–1600. https://doi.org/10.5194/gmd-12-1573-2019
Xin-Yao R, Jian L, Hao-Ming C, Yu-Fei X, Jing-Zhi S, Li-Juan H (2019) Introduction of CAMS-CSM model and its participation in CMIP6. Adv Clim Change Res 15: 540. https://doi.org/10.12006/j.issn.1673-1719.2019.186
Yang K, Guo X, Wu B (2011) Recent trends in surface sensible heat flux on the Tibetan Plateau. Sci China Earth Sci 54:19–28. https://doi.org/10.1007/s11430-010-4036-6
Yao Y, Liang S, Li X, Liu S, Chen J, Zhang X, Jia K, Jiang B, Xie X, Munier S (2016) Assessment and simulation of global terrestrial latent heat flux by synthesis of CMIP5 climate models and surface eddy covariance observations. Agric Meteorol 223:151–167. https://doi.org/10.1016/j.agrformet.2016.03.016
Yin J, Medellín-Azuara J, Escriva-Bou A, Liu Z (2021) Bayesian machine learning ensemble approach to quantify model uncertainty in predicting groundwater storage change. Sci Total Environ 769:144715. https://doi.org/10.1016/j.scitotenv.2020.144715
You Q, Cai Z, Wu F, Jiang Z, Pepin N, Shen SS (2021) Temperature dataset of CMIP6 models over China: evaluation, trend and uncertainty. Clim Dyn 57:17–35. https://doi.org/10.1007/s00382-021-05691-2
Zajaczkowski J, Wong K, Carter J (2013) Improved historical solar radiation gridded data for Australia. Environ Model Softw 49:64–77. https://doi.org/10.1016/j.envsoft.2013.06.013
Zhang S, Li X, She J (2020) Error assessment of grid-based terrain shading algorithms for solar radiation modeling over complex terrain. Trans GIS 24:230–252. https://doi.org/10.1111/tgis.12594
Zhou L-T, Du Z (2016) Regional differences in the surface energy budget over China: an evaluation of a selection of CMIP5 models. Theoret Appl Climatol 124:241–266. https://doi.org/10.1007/s00704-015-1407-0
Ziehn T, Chamberlain MA, Law RM, Lenton A, Bodman RW, Dix M, Stevens L, Wang Y-P, Srbinovsky J (2020) The Australian earth system model: ACCESS-ESM1. 5. J South Hemisphere Earth Syst Sci 70:193–214. https://doi.org/10.1071/ES19035